Folding of a donor–acceptor polyrotaxane by using noncovalent bonding interactions

Wenyu Zhang*, William R. Dichtel*†, Adam Z. Stieg*, Diego Benítez*, James K. Gimzewski*, James R. Heath†, and J. Fraser Stoddart*§

*California NanoSystems Institute and Department of Chemistry and Biochemistry, University of California, 405 Hilgard Avenue, Los Angeles, CA 90095; and †Division of Chemistry and Chemical Engineering, California Institute of Technology, 1200 East California Boulevard, Pasadena, CA 91125

Edited by Jack Halpern, University of Chicago, Chicago, IL, and approved February 26, 2008 (received for review November 21, 2007)

Mechanically interlocked compounds, such as bistable catenanes and bistable rotaxanes, have been used to bring about actuation in nanoelectromechanical systems (NEMS) and molecular electronic devices (MEDs). The elaboration of the structural features of such rotaxanes into macromolecular materials might allow the utilization of molecular motion to impact their bulk properties. We report here the synthesis and characterization of polymers that contain π electron-donating 1,5-dioxynaphthalene (DNP) units encircled by cyclobis(paraquat-*p*-phenylene) ($CBPQT^{4+}$), a π electron-accepting tetracationic cyclophane, synthesized by using the copper(I)-catalyzed azide-alkyne cycloaddition (CuAAC). The polyrotaxanes adopt a well defined ''folded'' secondary structure by virtue of the judicious design of two DNP-containing monomers with different binding affinities for $CBPQT^{4+}$. This efficient approach to the preparation of polyrotaxanes, taken alongside the initial investigations of their chemical properties, sets the stage for the preparation of a previously undescribed class of macromolecular architectures.

click chemistry | foldamers | polymers | supramolecular chemistry | rotaxanes

The design of polymeric materials incorporating broad-scale, electromechanical motion such as those associated with electrochemically switchable, bistable [2]rotaxanes (1, 2) and bistable [2]catenanes (3, 4) might allow these nanoscopic phenomena to be harnessed and to impact macroscopic properties. New classes of processable materials, potentially capable of bulk actuation (5), the stimulus-driven release of therapeutics (6), or stimuli-responsive changes in wettability or electronic properties (7) will result. Linear polyrotaxanes are one such architecture of interest, with relatively few reported examples except for those using cyclodextrin (8) or cucurbituril (9) derivatives as the macrocyclic component. Polyrotaxanes based on donor–acceptor binding interactions, and featuring cyclobis(paraquat-*p*-phenylene) ($CBPQT^{4+}$) as the π-accepting ring component, are highly desirable targets because its redox-controlled electromechanical motions have already been used in a range of nanoelectromechanical systems (NEMS) (2) and molecular electronic devices (MEDs) (10–12).

Such donor–acceptor polyrotaxanes have, thus far, been synthetically elusive, mostly because the template-directed "clipping" methodology used traditionally for the installation of $CBPQT^{4+}$ rings is not efficient enough to obtain a high coverage of macrocycles encircling the polymer backbone. We recently developed, however, a "threading-followed-by-stoppering" protocol for the synthesis of donor–acceptor rotaxanes (13) and catenanes (14), which takes advantage of the high efficiency and excellent functional group tolerance of the Cu(I)-catalyzed azide–alkyne cycloaddition (CuAAC) (15, 16). Inspired by the growing use of this transformation for polymer synthesis and functionalization (17, 18), we have adapted this "click chemistry" approach to the synthesis of high-molecular-mass polymers containing π electron-donating 1,5-dioxynaphthalene (DNP) units along the polymer chain. Thereafter, $CBPQT^{4+}$ rings were threaded onto the chains and bulky stoppers were attached, employing the CuAAC reaction once again.

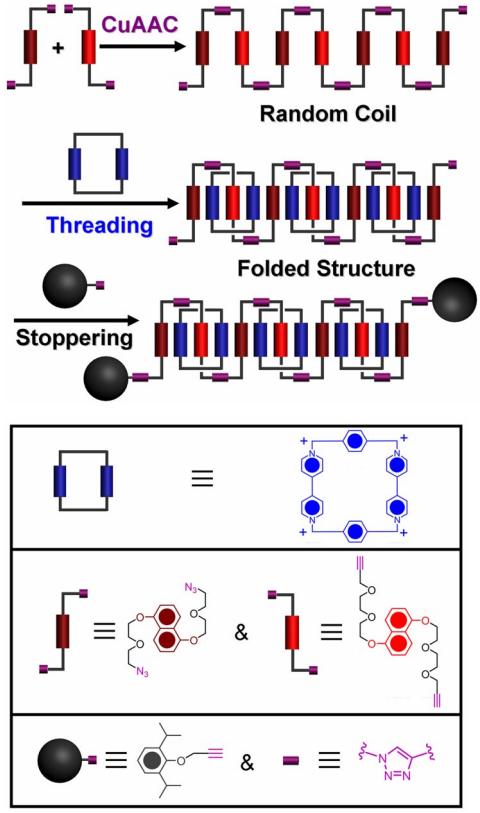

Fig. 1. Schematic representation of the formation of polymer thread and the polyrotaxane from two DNP-containing monomers.

One of the first unique properties observed in these polyrotaxanes is that they fold into a compact structure as a consequence of secondary intramolecular interactions. By virtue of the alternating nature of the A–A + B–B polymerization, in concert with the judicious design of the two DNP-containing monomers with differing binding affinities for $CBPQT^{4+}$, a majority of the rings encircle the more favorable DNP recognition site, whereas the secondary DNP recognition sites stack on the outside of the rings.

Author contributions: W.Z., W.R.D., A.Z.S., D.B., J.K.G., J.R.H., and J.F.S. designed research; W.Z., W.R.D., A.Z.S., and D.B. performed research; and W.Z., W.R.D., A.Z.S., D.B., J.K.G., J.R.H., and J.F.S. wrote the paper.

The authors declare no conflict of interest.

This article is a PNAS Direct Submission.

§To whom correspondence should be sent at the present address: Department of Chemistry, Northwestern University, 2145 Sheridan Road, Evanston, IL 60208. E-mail: stoddart@northwestern.edu.

This article contains supporting information online at www.pnas.org/cgi/content/full/0711072105/DCSupplemental.

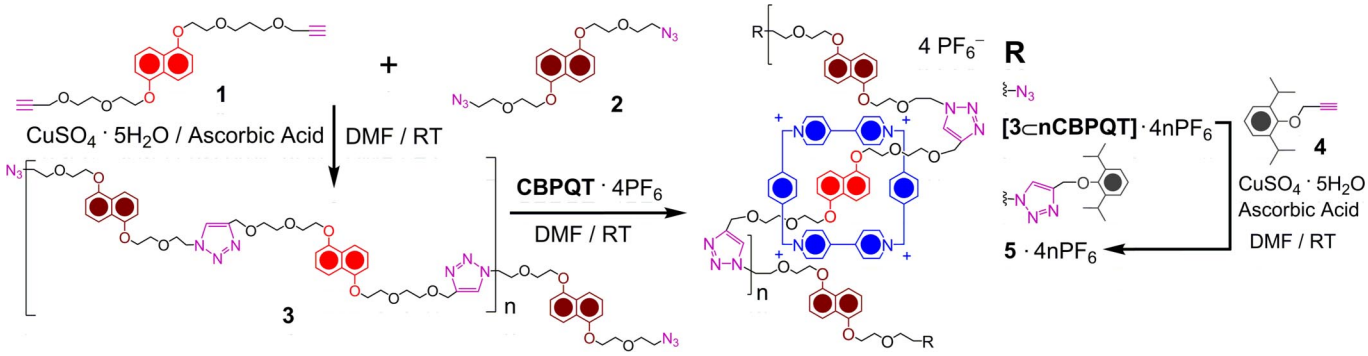

Scheme 1. Reaction scheme illustrating the synthesis of the polyrotaxane 5·4nPF$_6$.

In this manner, the polymer adopts a folded conformation (Fig. 1) in a fashion reminiscent of the pleated secondary structure adopted by polymers of alternating π electron donors and acceptors in aqueous solution (19). This folding behavior has also been observed in more rigid polymers and oligomers of certain polyamides (20), as well as in *m*-phenylene ethylene (21) "foldamers" (22–25).

Synthetic Investigations

The two monomers used for the synthesis of the polymer thread are each derivatives of 1,5-bis(2-(2-hydroxyethoxy)ethoxy)naphthalene (BHEEN). Their differing binding affinities toward CBPQT^{4+} are a direct consequence of their terminal substitution: the propargyl ether-terminated glycol chains of **1** contain an extra oxygen atom relative to the diazide-terminated (26) diethylene glycol chains of **2**. These oxygen atoms are key for the [C–H···O] interactions that strengthen the CBPQT^{4+}–DNP complex (27, 28). The CuAAC polymerization was carried out (Scheme 1) by using a mixture of the two monomers in the presence of 0.05 equivalents of $CuSO_4$·$5H_2O$ and 0.1 equivalent of ascorbic acid in DMF at room temperature. The number-average degree of polymerization X_n was controlled by employing a slight stoichiometric imbalance in the feed ratio of the two monomers, *r*, as described by Eq. **1** (29).

$$\bar{X}_n = \frac{N_A\left(1+\frac{1}{r}\right)/2}{[N_A(1-p)+N_B(1-rp)]/2} = \frac{1+r}{1+r-2rp}, \qquad [1]$$

$$r = \frac{N_A}{N_B}.$$

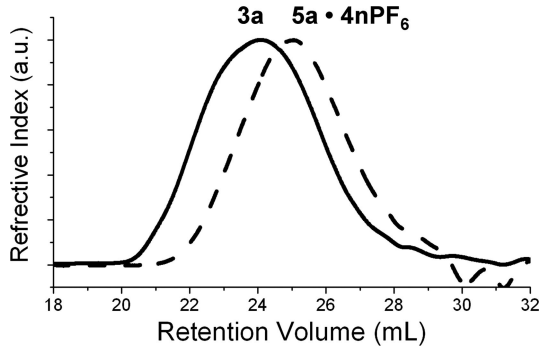

Fig. 2. Gel permeation chromatographs of the polymer thread 3a and polyrotaxane 5a·4nPF$_6$. Although the molecular mass of 5a·4nPF$_6$ is nearly twice that of 3a, the retention volume of the polyrotaxane increases, a phenomenon attributed to its folded structure. Comparisons between polymer threads 3b and 3c and polyrotaxanes 5b·4nPF$_6$, 5c·4nPF$_6$, respectively, showed the same trend [see Table 1 and supporting information (SI) Fig. S1].

We varied the ratio of the two DNP-containing monomers to obtain (Table 1) polymers with different molecular mass—namely, 32 kDa, 53 kDa, and 181 kDa, respectively. In the case of polymers **3a** and **3b**, the diazide monomer **2** was used in excess to ensure that the polymer chains would be terminated with azides. For the largest polymer **3c**, equimolar amounts of **1** and **2** were used during the polymerization. However, excess of **2** was added, along with more $CuSO_4$·$5H_2O$ and ascorbic acid after the polymerization was complete, to ensure the fidelity of the end groups. These polymerizations yielded a series of high-molecular-mass polymers with polydispersity indices (PDIs) ranging from 1.71–1.90 (Table 1 and Fig. 2). These results are consistent with the expected step-growth polymerization mechanism, although lower PDIs have been observed for some polymers prepared by using A–A + B–B CuAAC polymerizations (30).

When 0.6 equivalents of CBPQT^{4+} relative to the total number of DNP units was added to solutions of the polymer threads **3a–c**, the characteristic charge-transfer absorption band at 485 nm was observed by UV/Vis spectroscopy, a phenomenon that indicates the formation of the pseudopolyrotaxane [**3**⊂nCBPQT]·4nPF$_6$. The UV/Vis spectra of these solutions changed continually over the course of 24 h, after which time they ceased to change. These observations suggest that the threading process occurs slowly, an observation that was not surprising at all to us. Threading may occur only at the chain ends and previously threaded tetracationic cyclophanes presumably must migrate to the interior of the chains to free more unoccupied DNP units near the ends of the chains to bind additional rings. Finally, bulky 2,6-diisopropylphenyl stoppers were attached to the chain ends by using the CuAAC reaction between the pseudopolyrotaxanes [**3**⊂nCBPQT]·4nPF$_6$ and the stopper **4**, mechanically locking the dynamic pseudopolyrotaxanes and converting them into the corresponding polyrotaxanes **5a–c**·4nPF$_6$. The progress of the stoppering reaction was monitored by IR spectroscopy by observing the disappearance of the azide endgroup stretch at 2103 cm^{-1} (see Fig. S2). When stoppering was complete, the polymers were precipitated into aqueous EDTA solutions to remove the Cu catalyst, and the majority of unthreaded CBPQT^{4+} was removed by filtering the solution

Table 1. Gel permeation chromatography (GPC) of polymer thread 3(a–c) and polyrotaxane 5(a–c)·4nPF$_6$ (in parentheses)

Polymer sample	N_{alkyne}/N_{azide}	Retention volume, ml	Polydispersity index	M_n, kDa
3a (5a)	0.905	24.1 (25.0)	1.90	32
3b (5b)	0.975	23.3 (24.9)	1.78	53
3c (5c)	1.000	22.3 (23.3)	1.71	181

The number-average molecular masses (M_n) of 3(a–c) were determined by multiangle light scattering.

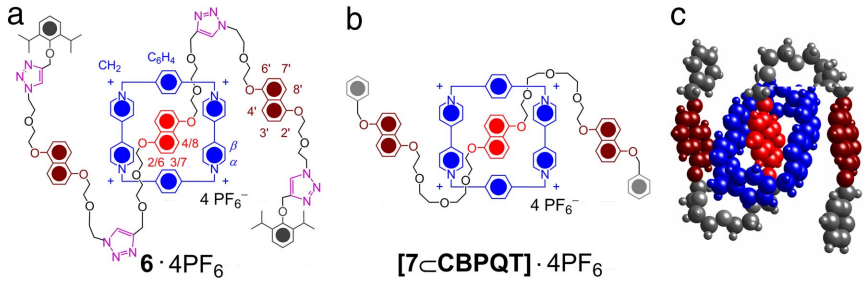

Fig. 3. Structural formula for the [2]rotaxane **6**·4PF_6 (*a*), the [2]pseudorotaxane [**7**⊂CBPQT]·4PF_6 (*b*), and the x-ray crystal structure of [**7**⊂CBPQT]$^{4+}$ (*c*).

through a DNP-functionalized PS-coDVB cross-linked resin. Finally, the polyrotaxanes were precipitated from DMF into $CHCl_3$ to remove unreacted monomers, low-molecular-mass oligomers and trace cyclic species. The coverage of CBPQT^{4+} rings into the polyrotaxanes was determined to be 90%, 74%, and 58% of CBPQT^{4+} per repeat unit for samples **5a–c**·4nPF_6, respectively, by ^{1}H NMR spectroscopy, as a result of comparing the integration of the CBPQT^{4+} α-proton resonances with those of the collective glycol methylene resonances of the polymer backbone found between 3.0 and 5.0 ppm (see Fig. S4).

Results and Discussion

Polymer Characterization. Gel permeation chromatography (GPC) analysis of the polyrotaxanes suggests that the polyrotaxanes **5a–c**·4nPF_6 exhibit smaller hydrodynamic volumes than their direct synthetic precursors **3a–c**. For example, the retention volume (Fig. 2) of **5a**·4nPF_6 (25.0 ml) is larger than that of **3a** (24.1 ml). Similar results were obtained (Table 1 and Fig. S1) for the retention volumes of the polymer threads **3b** and **3c** and the polyrotaxanes **5b**·4nPF_6 and **5c**·4nPF_6, respectively. These observations were particularly surprising because the addition of one CBPQT^{4+} ring per two DNP units would almost double the molecular mass of the polymer. This shift to higher retention volume is, however, consistent with the formation of a folded polymer conformation. This phenomenon is well known in the comparison of GPCs of globular dendrimers (31) compared with linear polymers of similar molecular mass and in intramolecularly cross-linked polymer chains (32).

Folding of Oligomeric Model Compounds. A series of ^{1}H NMR spectroscopic studies on a model [2]rotaxane **6**·4PF_6 (Fig. 3*a*) sheds some light on the folding behavior of the polyrotaxanes. The [2]rotaxane is a model compound for the polyrotaxane **5**·4nPF_6 in which $n = 1$. It is also a triazole-containing analogue of the [2]pseudorotaxane [**7**⊂CBPQT]·4PF_6 (Fig. 3*b*) composed of a linear tri-DNP thread and a CBPQT^{4+} macrocycle, which has been shown (33) to fold into a similar π-stacked structure. This folding is quite apparent in the solid-state superstructure (Fig. 3*c*) of the complex, in which the π electron-donating CBPQT^{4+} encircles the middle DNP unit, and the other two DNP units stack on the outside of the tetracationic cyclophane, maximizing the donor–acceptor interactions by forming a five-layer, π-stacked donor–acceptor system.

The ^{1}H NMR spectra of the polyrotaxane **5c**·4nPF_6 and the model [2]rotaxane **6**·4PF_6 are quite similar (Table 2 and Table S1) to those reported (33) for the [2]pseudorotaxane [**7**⊂CBPQT]·4PF_6, suggesting that the CuAAC-derived compounds adopt a very similar folded secondary structure. In the spectrum (Fig. 4*a*) of **6**·4PF_6 recorded at 245 K, the α-CH, β-CH, and *N*-methylene protons signals of the CBPQT^{4+} ring, are shifted upfield ($\Delta\delta$ = 0.33–1.54 ppm) relative to free CBPQT^{4+}, as expected when the cyclophane is encircling a DNP unit. Each of the signals is split into two resonances, and this observation, combined with the overall symmetry of the spectrum, is suggestive of a structure in which the local symmetry is C_{2h}, with the CBPQT^{4+} located on the middle DNP unit. The signals of the central DNP proton resonances (H-2/6, H-3/7 and H-4/8) were shifted upfield ($\Delta\delta$ = 1.12–5.97

Table 2. Selected induced 500-MHz ^{1}H NMR chemical shift changes for the [2]pseudorotaxane [7⊂CBPQT]·4PF_6, the [2]rotaxane 6·4PF_6, and polyrotaxane 5c·4nPF_6 in CD_3CN solution

	[2]Pseudorotaxane [7⊂CBQT]·4PF_6			[2]Rotaxane 6·4PF_6			Polyrotaxane 5c·4nPF_6
Proton	δ_{uc}	δ_c (243 K)	$\Delta\delta$	δ_{uc}	δ_c (245 K)	$\Delta\delta$	δ_c (245 K)
CBPQT^{4+}							
α-CH	8.86	8.68	−0.18	8.86	8.50	−0.36	8.45
		8.12	−0.74		8.25	−0.61	8.19
β-CH	8.16	6.63	−1.53	8.16	6.79	−1.37	6.73
		6.57	−1.59		6.62	−1.54	6.55
DNP							
Alongside H-4′	7.77	7.32	−0.45	7.76	7.12	−0.64	7.23
Alongside H-8′	7.79	7.33	−0.46	7.79	7.38	−0.41	
Alongside H-7′	7.34	7.16	−0.18	7.38	7.27	−0.11	7.10
Alongside H-3′	7.32	7.07	−0.25	7.35	7.01	−0.34	
Alongside H-6′	6.88	6.69	−0.17	6.89	6.74	−0.15	6.54
Alongside H-2′	6.82	6.40	−0.42	6.88	6.56	−0.32	

δ_{uc} is the chemical shift in the spectrum of the protons of each component in the unencircled state at 245 K. δ_c is the chemical shift of the protons observed in the encircle systems. $\Delta\delta = \delta_c = \delta_{uc}$. The data for [2]pseudorotaxane [**7**⊂CBPQT]·4PF_6 are cited from ref. 33. A complete list of chemical shifts is shown in Table S1.

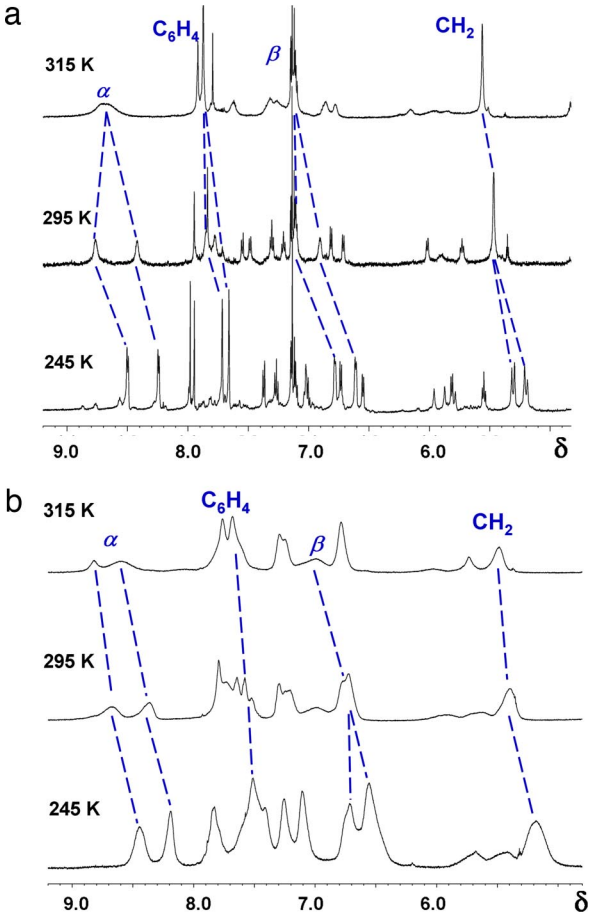

Fig. 4. VT ^{1}H NMR spectroscopic studies. (*a*) The [2]rotaxane **6**·4PF$_6$. Separate groups of α, β, and C_6H_4 protons are distinguishable at room temperature and below. Further sharpening of the peaks and splitting caused by coupling are observed when the sample is cooled down to 245 K. (*b*) The polyrotaxane **5**·4nPF$_6$. The spectrum of polyrotaxane has peaks with chemical shifts identical to those reported for the [2]rotaxane **6**·4PF$_6$. Coalescence of peaks is also observed while warming up the sample.

ppm) to a degree diagnostic for CBPQT^{4+} binding. Furthermore, the alongside DNP protons (H-2′ − H-4′, H-6′ − H-8′) exhibit six distinct signals, each shifted upfield to a smaller extent ($\Delta\delta$ = 0.11–0.64 ppm) than those of the central unit. The assignment of all of the above protons were also confirmed (Fig. S3) by COSY ^{1}H NMR spectroscopy at 245 K. The shifts of these resonances to higher field are attributed to the secondary donor–acceptor interactions that cause the alongside DNP units to stack on the outside of the CBPQT^{4+} rings. Thus, the direct comparison of the symmetry and magnitude of the chemical shifts in the [2]rotaxane **6**·4PF$_6$ and the [2]pseudorotaxane [**7**⊂CBPQT]·4PF$_6$ suggests that they fold in similar ways.

The polyrotaxane **5**·4nPF$_6$ displayed very similar NMR spectra (Fig. 4*b*) when compared with those of [2]rotaxane **6**·4PF$_6$(Fig. 4*a*). Protons on the CBPQT^{4+} ring, and on the included DNP unit, exhibit almost identical chemical shifts and splitting patterns to those observed for model compounds. In the polymer constitution, there is little difference in chemical environment between H-2′ and H-6′, H-3′ and H-5′, and H-4′ and H-8′, respectively, alongside the DNP units, and so these resonances are not split into individually assignable peaks as in the models **6**·4PF$_6$ and [**7**⊂CBPQT]·4PF$_6$. With the exception of this difference, the ^{1}H NMR spectrum of the polyrotaxane recorded at 245 K is quite similar to that of the [2]rotaxane **6**·4PF$_6$, exhibiting the

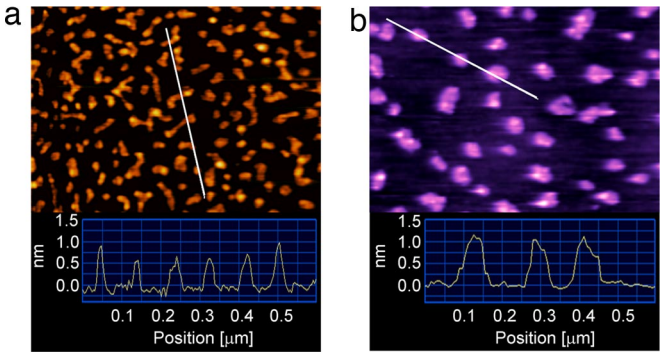

Fig. 5. Representative AFM height images of polymer thread (*a*), polyrotaxane (*b*), and cross-sectional linescans (*Insets*) on HOPG. Scan parameters: size,1 μm^2; scan rate, 0.5 Hz.

same splittings for the CBPQT^{4+} α-CH, β-CH, aromatic C_6H_4, and methylene proton resonances, as well as changes in the chemical shifts of the included in and alongside the DNP residues that are indicative of the folded conformation.

VT NMR spectroscopy was also used to probe the relative stabilities of the folded nature of the model and the polymer (34). At higher temperatures, the unfolding and subsequent refolding process becomes rapid on the NMR time-scale, resulting in the coalescence of the CBPQT^{4+} α-CH, β-CH, aromatic C_6H_4 and methylene proton resonances. The activation barrier for this process is therefore a measure of the relative stability of the folded conformation (35). Observation of the coalescence of signals arising from the CBPQT^{4+} α-CH, β-CH, aromatic C_6H_4 protons in the spectra of **6**·4PF$_6$ (Table S2) afforded an average value for the activation barrier of 12.0 kcal·mol^{-1}, indicating that the folded structure is somewhat less kinetically stable than in [**7**⊂CBPQT]·4PF$_6$, whose $\Delta G^{\ddagger}$ value is 14.7 kcal mol^{-1}. Interestingly, in the spectra of the polyrotaxanes **5**·4nPF$_6$,the signals for the α-CH protons at 8.2–8.7 ppm and the β-CH protons at 6.6–6.9 ppm, respectively, did not coalesce, even when the solution was heated to 335 K, i.e., just below the lower critical solution temperature of the polymer. This observation points to a cooperative effect in the thermal stability of the folded structure of the polymeric system. In the semicontinuous π–π stacked folded structure hypothesized for the polyrotaxane, the process by which these resonances interconvert most likely requires the simultaneous unfolding of two or more folded units, a much more energy-intensive process than the unfolding process in a [2]rotaxane.

Atomic Force Microscopy. The application of atomic force microscopy (AFM) (36) to the observation of individual polymer molecules enables real-space imaging of structural changes resulting from polymer folding (37–39). Measurements of both the polymer thread and polyrotaxane have revealed distinct differences in the appearance and overall dimensionality through cross-sectional analyses. Fig. 5 provides representative AFM images of both **3c** and **5c**·4PF$_6$ after deposition onto highly ordered pyrolytic graphite (HOPG). Optimization of the deposition conditions was carried out to minimize intermolecular interactions and produced samples with

Table 3. Observed relative dimension changes resulting from the folding process

	Δ %*L*	Δ %*W*	Δ %*H*
3c → **5c**·4nPF$_6$	(−)15.64	92.06	43.18

Negative values, denoted by (−) represent a decrease in measured molecular dimensions.

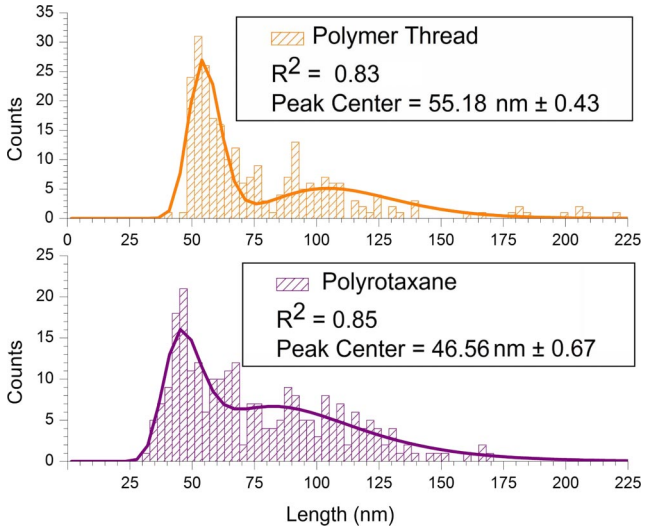

Fig. 6. Histogram and fitting results of measured molecular lengths from cross-sectional analyses demonstrating a decrease in structural length upon folding.

mostly isolated structural units. The determination of these observed structures as single molecules was carried out through the use of cross-sectional heights, as shown in the respective insets illustrated at the bottom of Fig. 5 *a* and *b*.

Variations in the observed feature length of the polyrotaxane, compared with the polymer thread, provide further evidence for the folding phenomenon. Specifically, a decrease in length and corresponding increase in both height and width for the polyrotaxane were observed (Table 3). The decrease in length and increase in width can be attributed to the longitudinal compression of the polymer chain and transverse structural broadening expected in the folding process (40). An increase in the measured height is attributed to the addition of $CBPQT^{4+}$ rings along the backbone of the polyrotaxane. Statistical analyses of height and width values from multiple samples, images, and tips determined the two systems to be statistically different to a 99.995% confidence level by using the two-sample *t* test. The single atomic step height of HOPG was used as an additional calibration in height measurements. Because of large standard deviations, compiled data were plotted as a histogram and fitted by using nonlinear least-squares analysis for increased accuracy. This type of presentation of the data was especially useful in the analysis of the molecular lengths, which exhibited a bimodal structure (Fig. 6 and Table S3) in the plotted histogram and was not readily represented by a simple mean value.

The observed variation in molecular dimensions compared with expected values from structural modeling and crystallography, can be attributed to image convolution resulting from both the finite radius of the probe tip and loading force applied to the sample to maintain stable, controlled feedback (41).

Conclusions

In summary, we synthesized DNP–$CBPQT^{4+}$-based polyrotaxanes, using the CuAAC, first for a step-growth polymerization of two different DNP units and then for the final stoppering step in the threading-followed-by-stoppering process that serves to constrain the $CBPQT^{4+}$ rings in the dumbbell component of the polyrotaxane. The polyrotaxanes adopt an alternating stacking pattern that is induced by secondary noncovalent bonding interactions between the rings and the alongside DNP units. GPC studies show that the folding causes a significant decrease in the polymer dimensions despite a near twofold molecular mass increase—a unique phenomenon that sets the polyrotaxane apart from traditional polymeric materials. The folding behavior was also confirmed by ^{1}H NMR spectroscopy by comparing the polyrotaxanes with a simple folded [2]rotaxane model compound. Moreover, analysis of individual polymer chains dispersed on HOPG by AFM indicates that the polyrotaxanes exhibit increased height and width but decreased lengths compared with the precursor threads, a result that is consistent with the other characterization methods. This research provides a strategy for the controllable fabrication of materials with elaborate structures at the nanometer-scale level. Directions for the research to take in the future could include the development of switchable polymeric systems incorporating multiple recognition units, which might find uses in nanoelectromechanical systems (NEMS) and molecular electronic devices (MEDs).

Materials and Methods

Chemicals were purchased from commercial suppliers and were used as received. BHEEN (27), bis(2-(2-azidoethoxy)ethoxy)-naphthalene (13), $CBPQT{\cdot}4PF_6$ (27) were prepared according to literature procedures. Gel permeation chromatography (GPC) was carried out on 15-μm columns set up in series with two linear mixed beds, followed by a 100-Å column. A 0.5 M solution of NH_4PF_6 in DMF was used as the mobile phase at 0.500 ml/min flow from an Agilent 1100 isocratic pump. The detector system consisted of a miniDawn three angle, light-scattering system, followed downstream by an Optilab Rex differential refractometer from Wyatt Technologies. Number-average molecular mass (M_n), weight-average molecular mass (M_w) and polydispersities (PDI = M_w/M_n) were determined relative to linear polystyrene (GPC_{PSt}). ^{1}H and ^{13}C NMR spectra were recorded on a Bruker DRX500 (500 MHz) or AV600 (600 MHz) spectrometer, with the residual solvent resonance as the internal standard. Infrared (IR) spectra were measured on a Perkin–Elmer 100 FT/IR spectrometer by using AgCl plates as the sample window. Electrospray ionization (ESI) mass spectra were measured on an Ionspec Fourier Transfer HiRes ESI Mass Spectrometer by using MeCN as the mobile phase. Electron ionization (EI) mass spectra were measured on a Shimadzu QP2010S GC-EI Mass Spectrometer. Fast atom bombardment mass spectra (FAB) were obtained on a JEOL JMS-600H high-resolution mass spectrometer equipped with a FAB probe.

General Polymerization Procedure. Polymer Thread **3**: Monomers **1** (290 mg, 702 mmol) and **2** (**3a**, **1**:**2** = 0.905:1; **3b**, **1**:**2** = 0.975:1; **3c**, **1**:**2** = 1:1), ascorbic acid (27.3 mg, 0.155 mmol) and $CuSO_4{\cdot}5H_2O$ (19.4 mg, 0.0776 mmol) were dissolved in DMF (4 ml). The mixture was stirred under argon for 24 h. In the case of **3c**, another 3 mg of **2** was added to the solution along with 0.1 mg of ascorbic acid and 0.1 mg of $CuSO_4{\cdot}5H_2O$, and the reaction mixture was stirred for an additional 3 h. The mixture was then added dropwise to an aqueous EDTA solution (0.1 M, 20 ml), forming a yellow precipitate. The precipitate was collected by centrifugation before being washed with H_2O (20 ml times two) and dried under high vacuum. The resulting solid was dissolved in CH_2Cl_2 (2 ml) and precipitated into Me_2CO (20 ml) to give the product. The solid was again recovered by centrifugation and finally dried under high vacuum. ^{1}H NMR (500 MHz, $CDCl_3$): δ = 8.08–8.04 (m, 2H, Triazole-**H**), 7.84–7.71 (m, 4H, Ar-$\mathbf{H^{2/6}}$), 7.42–7.30 (m, 4H, Ar-$\mathbf{H^{3/7}}$), 7.05–6.84 (m, 4H, Ar-$\mathbf{H^{4/8}}$), 4.61–3.60 (m, 32H, $\mathbf{CH_2}$O), 3.50–3.42 (m, 4H, $\mathbf{CH_2}$-Triazole).

Synthesis of Polyrotaxane 5·4nPF$_6$. A solution of $CBPQT{\cdot}4PF_6$ (48.1 mg, 0.0437 mmol) and polymer thread **3** (29.1 mg, N_{DNP} = 0.0728 mmol) in DMF (2 ml) was stirred at room temperature for 24 h. A purple solution indicative of pseudopolyrotaxane [**3**⊂n$CBPQT$]·$4nPF_6$ formation resulted. Stock solutions containing stopper **4** (1.6 mg, 0.00725 mmol), ascorbic acid (0.1 mg, 0.000726 mmol), and $CuSO_4{\cdot}5H_2O$ (0.1 mg, 0.000363 mmol), were then added to the solution. The reaction mixture was stirred under Ar at room temperature overnight. Resin-supported DNP **S6** (see *SI Text*) was added to the solution for 10 min before being removed by filtration. The solution was then added to an aqueous EDTA solution (0.1 M, 5 ml), forming a purple precipitate. The precipitate was recovered by centrifugation, washed with H_2O (5 ml times two) and dried under high vacuum for 2 h. The solid was dissolved in a minimum amount of DMF and precipitated when added to $CHCl_3$ (5 ml). The resulting polyrotaxane was again recovered by centrifugation and dried under vacuum. For further experimental details, see *SI Text* and Schemes S1-S5.

ACKNOWLEDGMENTS. Generous financial support by the Semiconductor Research Corporation through its focus centers of Functional Engineered NanoArchitectonics and Materials, Structures, and Devices in addition to the MolApps Program funded by the Defense Advanced Research Projects Agency is acknowledged gratefully.

1. Collier CP, *et al.* (2001) Molecular-based electronically switchable tunnel junction devices. *J Am Chem Soc* 123:12632–12641.
2. Liu Y, *et al.* (2005) Linear artificial molecular muscles. *J Am Chem Soc* 127:9745–9759.
3. Collier CP, *et al.* (2000) A [2]catenane based solid-state electronically reconfigurable switch. *Science* 289:1172–1175.
4. Liu Y, Klivansky LM, Khan SI, Zhang XY (2007) Templated synthesis of desymmetrized [2]catenanes with excellent translational selectivity. *Org Lett* 9:2577–2580.
5. Beebe DJ, *et al.* (2000) Functional hydrogel structures for autonomous flow control inside microfluidic channels. *Nature* 404:588–590.
6. Nguyen TD, *et al.* (2005) A reversible molecular valve. *Proc Natl Aca Sci USA* 102:10029–10034.
7. Berna J, *et al.* (2005) Macroscopic transport by synthetic molecular machines. *Nat Mater* 4:704–710.
8. Wenz G, Han BH, Müller A (2006) Cyclodextrin rotaxanes and polyrotaxanes. *Chem Rev* 106:782–817.
9. Whang D, Jeon YM, Heo J, Kim K (1996) Self-assembly of a polyrotaxane containing a cyclic ''bead'' in every structural unit in the solid state: Cucurbituril molecules threaded on a one-dimensional coordination polymer. *J Am Chem Soc* 118:11333–11334.
10. Steuerman DW, *et al.* (2004) Molecular mechanical switch-based solid-state electrochromic devices. *Angew Chem Int Ed* 43:6486–6491.
11. Chatterjee MN, Kay ER, Leigh DA (2006) Beyond switches: Ratcheting a particle energetically uphill with a compartmentalized molecular machine. *J Am Chem Soc* 128:4058–4073.
12. Fletcher SP, Dumur F, Pollard MM, Feringa BL (2005) A reversible, unidirectional molecular rotary motor driven by chemical energy. *Science* 310:80–82.
13. Dichtel WR, Miljanić OŠ, Spruell JM, Heath JR, Stoddart JF (2005) Efficient templated synthesis of donor-acceptor rotaxanes using click chemistry. *J Am Chem Soc* 128:10388–10390.
14. Miljanić OŠ, Dichtel WR, Mortezaei S, Stoddart JF (2006) Cyclobis(paraquat-*p*-phenylene)-based [2]catenanes prepared by kinetically controlled reactions involving alkynes. *Org Lett* 8:4835–4838.
15. Tornoe CW, Christensen C, Meldal M (2002) Peptidotriazoles on solid phase: [1,2,3]-triazoles by regiospecific copper(I)-catalyzed 1,3-dipolar cycloadditions of terminal alkynes to azides. *J Org Chem* 67:3057–3064.
16. Rostovtsev VV, Green LG, Fokin VV, Sharpless KB (2002) A stepwise Huisgen cycloaddition process: Copper(I)-catalyzed regioselective ''ligation'' of azides and terminal alkynes. *Angew Chem Int Ed* 41:2596–2599.
17. Lutz JF (2007) 1,3-Dipolar cycloadditions of azides and alkynes: A universal ligation tool in polymer and materials science. *Angew Chem Int Ed* 46:1018–1025.
18. Hawker CJ, Wooley KL (2005) The convergence of synthetic organic and polymer chemistries. *Science* 309:1200–1205.
19. Lokey RS, Iverson BL (1995) Synthetic molecules that fold into a pleated secondary structure in solution. *Nature* 375:303–305.
20. Appella DH, *et al.* (1997) Residue-based control of helix shape in β-peptide oligomers. *Nature* 387:381–384.
21. Hill DJ, Moore JS (2002) Supramolecular chemistry and self-assembly special feature: Helicogenicity of solvents in the conformational equilibrium of oligo(*m*-phenylene ethynylene)s: Implications for foldamer research. *Proc Natl Acad Sci USA* 99:5053–5057.
22. (2007) In *Foldamers—Structure, Properties, and Applications*, eds Hecht S, Huc I (Wiley–VCH, Weinheim, Germany).
23. Estroff LA, Incarvito CD, Hamilton AD (2004) Design of a synthetic foldamer that modifies the growth of calcite crystals. *J Am Chem Soc* 126:2–3.
24. Buffeteau T, Ducass, L, Poniman L, Delsuc N, Huc I (2006) Vibrational circular dichroism and *ab initio* structure elucidation of an aromatic foldamer. *Chem Commun* 2714–2716.
25. Khan A, Kaiser C, Hecht S (2006) Prototype of a photoswitchable foldamer. *Angew Chem Int Ed* 45:1878–1881.
26. Bräse S, Gil C, Knepper K, Zimmermann Z (2004) Organic azides: An exploding diversity of a unique class of compounds. *Angew Chem Int Ed* 44:5188–5240.
27. Venturi M, Dumas S, Balzani V, Cao JG, Stoddart JF (2004) Threading/dethreading processes in pseudorotaxanes. A thermodynamic and kinetic study. *New J Chem* 28:1032–1037.
28. Anelli PL, *et al.* (1992) Molecular Meccano 1. [2]Rotaxanes and a [2]catenane made to order. *J Am Chem Soc* 114:193–218.
29. Odian GG (1991) in *Principles of Polymerization* (Wiley, New York), pp 41–90.
30. Srinivasachari S, Liu YM, Zhang GD, Prevette L, Reineke TM (2006) Trehalose click polymers inhibit nanoparticle aggregation and promote pDNA delivery in serum. *J Am Chem Soc* 128:8176–8184.
31. Fréchet JMJ (1994) Functional polymers and dendrimers: Reactivity, molecular architecture, and interfacial energy. *Science* 263:1710–1715.
32. Harth E, *et al.* (2002) The effect of macromolecular architecture in nanomaterials: A comparison of site isolation in porphyrin core dendrimers and their isomeric linear analogues. *J Am Chem Soc* 124:8653–8660.
33. Amabilino DB, *et al.* (1995) Molecular meccano 3: Constitutional and translational isomerism in [2]catenanes and [n]pseudorotaxanes. *J Am Chem Soc* 117:11142–11170.
34. Vignon SA, Stoddart JF (2005) Exploring dynamics and stereochemistry in mechanically interlocked compounds. *Coll Czech Chem Commun* 70:1493–1576.
35. Sutherland IO (1971) Investigation of the kinetics of conformational changes by nuclear magnetic resonance spectroscopy. *Annu Rep NMR Spectrosc* 4:71–235.
36. Binnig G, Quate CF, Gerber C (1986) Atomic force microscope. *Phys Rev Lett* 56:930–933.
37. Kumaki J, Nishikawa Y, Hashimoto T (1996) Visualization of single-chain conformations of a synthetic polymer with atomic force microscopy. *J Am Chem Soc* 118:3321–3322.
38. Sheiko S, Möller M (2001) Visualization of macromolecules—a first step to manipulation and controlled response. *Chem Rev* 101:4099–4123.
39. Kim Y, Pyun J, Fréchet JMJ, Hawker CJ, Frank CW (2005) The dramatic effect of architecture on the self-assembly of block copolymers at interfaces. *Langmuir* 21:10444–10458.
40. Börner HG, Beers K, Matyjaszewski K, Sheiko SS, Möller M (2001) Atomic-force microscopy of gel-drawn ultrahigh-molecular-weight polyethylene. *Macromolecules* 34:4375–4386.
41. Magonov SN (2001) Visualization of polymers at surfaces and interfaces with atomic force microscopy. *Handbook of Surfaces and Interfaces of Materials*, ed Nalwa HR (Academic, New York), Vol 2, pp 393–429.